J. Fluid Mech. (2005), *vol.* 542, *pp.* 115–137.
doi:10.1017/S0022112005006385 Printed in the United Kingdom

An experimental study of the oscillatory flow structure of tone-producing supersonic impinging jets

By BRENDA HENDERSON[1], JAMES BRIDGES[2] AND MARK WERNET[2]

[1]NASA Langley Research Center, Hampton, VA 23681, USA

[2]NASA Glenn Research Center, 21000 Brookpark Road, Cleveland, OH 44135, USA

(Received 8 January 2004 and in revised form 2 June 2005)

An experimental investigation into the structure of a supersonic jet impinging on a large plate is presented. Digital particle image velocimetry (DPIV), shadowgraph photography and acoustic measurements are used to understand the relationship between the unsteady jet structure and the production of tones for nozzle-to-plate spacings between 1 and 5 nozzle exit diameters at a nozzle–pressure ratio equal to 4. Results indicate that the instability of the jet depends on the location of the plate in the shock cell structure of the corresponding free jet and the strength of the standoff shock wave, rather than on the occurrence of recirculation zones in the impingement region. Phase-locked studies show streamwise displacements of the stand-off shock wave, a moving recirculation zone in the subsonic flow in front of the plate, and significant oscillations of both the compression and expansion regions in the peripheral supersonic flow when tones are produced. Sound is shown to be generated by periodic pulsing of the wall jet boundary resulting from periodic motion of the flow in the impingement and near-wall regions of the flow.

1. Introduction

The impingement of a supersonic jet on a flat plate placed perpendicular to the jet axis produces very intense, discrete-frequency sound. The sound characteristics depend on the nozzle–pressure ratio (the ratio of the stagnation pressure to the pressure at the nozzle lip), the nozzle-to-plate spacing, and the impinging plate size. Although Henderson & Powell (1993) have shown that the tones are part of a feedback loop to the nozzle, the sound-production mechanism is not well understood owing to the complex nature of the oscillatory jet structure and the fluid–acoustic interactions. Previous investigators have reported shock-wave oscillations, recirculation zones in the impingement-region flow, and interactions between jet disturbances and shock waves (see Ginzburg *et al.* 1970; Nakatogawa, Hirata & Kukita 1971; Alvi & Iyer 1999; Henderson 2002). However, the relationship between these flow features and the production of sound is unclear. The intent of the present study is to understand better the connection between the periodic motion of the jet oscillations and the production of discrete-frequency sound.

Shock-wave oscillations, or shock-wave instabilities, have been observed for jets impinging on large plates (impinging plates with diameters in excess of 2 nozzle exit diameters). Nozzle–pressure ratio and plate location appear to have an effect

on the shock-wave instability. Nakatogawa *et al.* (1971) observed strong stand-off shock-wave oscillations when the stand-off shock wave was located in a decelerating region of the jet. Ginzburg *et al.* (1970) found strong stand-off shock oscillations when a recirculation zone occurred in front of the plate. The shock-wave oscillations observed by Semiletenko, Sobkolov & Uskov (1974) ceased when the nozzle-to-plate spacing became large enough that a second shock wave occurred in front of the plate. In Ginzburg, Semiletenko & Uskov (1975), strong shock-wave instability first occurred when the plate pressures at the centre of the plate became equal to that in the peripheral plate regions with any further increase in plate distance resulting in recirculation regions in front of the plate. It is clear that a relationship exists between the location of the plate in the jet structure and the occurrence of stand-off shock-wave oscillations. However, the connection between the oscillations of the shock wave and the production of discrete tones is not well understood.

Periodic shear-layer instabilities have been observed in the impinging jet experiments of Krothapalli *et al.* (1999), Elavarasan *et al.* (1999, 2002), Arunajatesan & Sinha (2002) and Henderson & Powell (1993). Although there appears to be a connection between these disturbances and the production of tones, attempts to model the sound source mechanism as one related to vortex acceleration (see Henderson 1993) have been unsuccessful, perhaps owing to the lack of interaction between the flow instabilities and the stand-off shock wave in this type of model.

Although recirculation zones have been observed for supersonic impinging jets, it is difficult to determine the importance of this phenomenon to the production of tones since these zones are observed for both steady and unsteady jets. The studies by Donaldson & Snedeker (1971), Carling & Hunt (1974), Gummer & Hunt (1974) and Kalghatgi & Hunt (1976) reported the occurrence of recirculation zones for stable impinging jets, and the plate pressure measurements of Alvi & Iyer (1999) indicate the occurrence of recirculation zones for nozzle-to-plate spacings where Henderson (2002) found no tonal production. Recirculation zones were also observed in the unstable impinging jet experiments performed by Ginzburg *et al.* (1970) and the numerical analysis of Iwamoto & Deckker (1981), although the numerical study was not carried to steady state so it was not possible to determine the final stability condition of the jet. Detailed digital particle image velocimetry (DPIV) studies and numerical models of the impinging region flow in the studies of Alvi, Ladd & Bower (2002) also reveal recirculation zones. However, only mean velocity and vorticity fields were presented and the stability condition of the jet was unclear in the reported results. Although Ginzburg *et al.* (1970) and Kalghatgi & Hunt (1976) have suggested a connection between flow instability and unsteady recirculation zones in front of the plate, the relationship between the occurrence of recirculation zones and the production of tones is unknown.

One-dimensional instability models have shed some light on the instability of the supersonic impinging jet although it has not been possible to recover large-plate frequencies from any of the analyses. Morch (1964) and Kuo & Dowling (1996) confined the flow resonance to the impingement region of the jet and considered shock-wave motion resulting from the propagation of sound waves in the region between the stand-off shock wave and the plate. Morch hypothesized that the failure of his model to produce a strong resonance condition was due to the two-dimensional nature of the flow that was not captured by the model. Morch (1973) modified his earlier analysis to include a composite jet in an attempt to introduce the effects of the flow in the peripheral regions of the jet. Kuo & Dowling (1996) extended Morch's original model by accounting for entropy waves in the stagnation flow

which resulted in a strong resonance condition. However, the calculated resonance frequencies matched those measured by Powell (1988) for small-plate tones although there was nothing in the model limiting the plate size. Small-plate tones have different frequency characteristics from those associated with impingement on large plates (see Powell 1988; Henderson & Powell 1996, 1997). Kuo & Dowling (1996) suggested that the analysis failed to produce large-plate impinging tones because the model lacked upstream forcing of the shock wave such as occurs for flows involving feedback to the nozzle. Henderson (2002) observed shock-wave oscillations and the periodic disappearance of the annular shock wave in the peripheral regions of the jet when strong discrete frequency tones were produced, an indication that the instability may be more complex than that described by simple one-dimensional instability models.

The sound-production mechanism of large-plate impinging tones is not well understood owing, in part, to the lack of information about the time-dependent flow in the impingement and near-wall regions of the jet. Time-dependent plate pressure measurements, limited stand-off shock-wave oscillation information from shadowgraph photographs, mean flow characteristics determined from DPIV studies, and some hot-wire data in the impingement region exist for very limited nozzle-to-plate spacings and nozzle–pressure ratios (NPR), where NPR is the ratio of the stagnation pressure to the pressure at the nozzle lip. Owing to differences in the operating conditions used in previous studies and the dependency of the flow characteristics on nozzle-to-plate spacing, NPR, and plate size, it has not been possible to develop a sound source model for the supersonic impinging jet. The occurrence of shock-wave oscillations, oscillating stagnation regions, shear-layer disturbances accelerating and decelerating in the impingement and near-wall regions of the jet, and the interaction of flow disturbances with the shock waves are all potential sources of sound. Additional studies should be performed to understand better the oscillatory flow structure of the supersonic impinging jet and gain insight into the sound-production mechanism of large-plate impinging tones.

In this investigation, a detailed study of the mean and time-dependent flow field of the underexpanded supersonic impinging jet is investigated with phase-delayed shadowgraph photography and DPIV. The importance of shock-wave oscillations and recirculation zones to the production of discrete tones will be explored. Finally, a sound-production mechanism for large-plate impinging tones will be presented. Portions of this work were presented in Henderson, Bridges & Wernet (2002).

2. Experimental methods

The experimental work was performed at the NASA Glenn Research Center (GRC) using the small hot jet aeroacoustics rig (SHJAR) located in the Aeroacoustic Propulsion Laboratory (AAPL). The AAPL is a 20 m radius geodesic dome with fibreglass wedges on the walls and approximately half of the floor area. A schematic of the rig is shown in figure 1. Air enters the rig at 1034 kPa through a 102 mm diameter line. The desired nozzle pressure ratio (NPR) is maintained with two low-noise control valves and a vernier valve. The flow passes through two 90° elbows then enters the 356 mm diameter plenum chamber instrumented with total pressure probes used to monitor NPR. An ASME bellmouth contraction passes the flow to a 152 mm diameter pipe containing three screens. The centreline of the SHJAR is located at approximately 3.05 m above the facility floor.

In the present studies, the flow exhausted from the SHJAR through a contoured convergent nozzle with a 25.4 mm exit diameter. The nozzle external contour was a

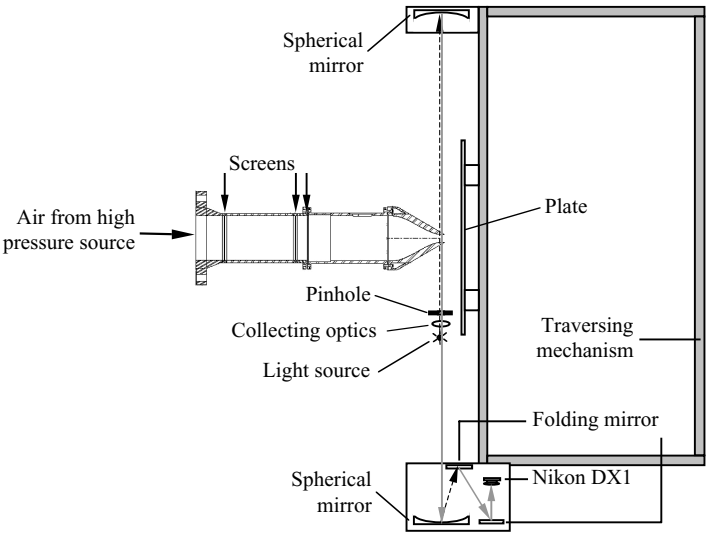

FIGURE 1. A plan view of the SHJAR at the NASA Glenn Research Center showing the location of the shadowgraph system components.

30° cone with a lip thickness of 1.27 mm. The flow impinged on a 533 mm × 610 mm aluminium plate located perpendicular to, and traversed along, the jet axis. Although a range of nozzle-to-plate spacings and NPR were used in the experiments, only the results for NPR equal to 4 (fully expanded Mach number equal to 1.55) and nozzle-to-plate spacings between 1.6 and 5 nozzle exit diameters are reported here.

A shadowgraph system was located on the plate traversing mechanism. A Photonics Analysis Pal Flash with a 1 μs spark duration was used as a light source. The light was focused on a pinhole then passed to a 508 mm diameter spherical mirror with a 2.54 m focal length. The parallel rays from the spherical mirror were passed to a second 508 mm diameter spherical mirror on the other side of the test section then focused onto a Nikon DX1 digital camera. Limited space on the optical stands and traversing mechanism made it necessary to use two folding mirrors on the camera side of the system. The signal from a Bruel and Kjaer type 4135, 6.35 mm diameter free-field microphone placed in the far field was used to trigger phase-locked shadowgraph photographs. The microphone signal was filtered at the frequency of the tone then time delayed with a Model DG 535 Stanford Research Digital Delay Generator. The output from the delay generator triggered the light source at the desired phase angle in the oscillation cycle.

The components for the DPIV studies were located on the traversing mechanism as shown in figure 2. A Continuum DPIV-Surelite III, 400 mJ per pulse at 532 nm, dual head, Nd:YAG laser produced light pulses with a 1.2 μs inter-frame time. A laser light sheet approximately 0.2 mm thick was formed with one cylindrical and one spherical lens. The light sheet was directed along the jet axis. A Redlake ES 4.0 digital camera with a 2048 × 2048 pixel CCD array was used to record the images. An 80 mm field of view was used for nozzle-to-plate spacings less than 75 mm and a 136 mm field of view was used for larger spacings. For the 80 mm field of view, the particle displacements ranged from 0 to 17 pixels resulting in a full-scale error of 1.2 % for a maximum measured velocity of 550 m s^{-1}. For the 136 mm field of view, the full-scale error was 2.0 %.

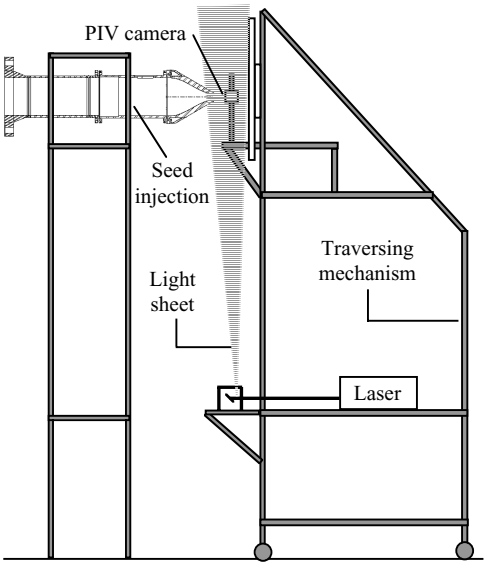

FIGURE 2. A schematic of the SHJAR showing the location of the DPIV system components.

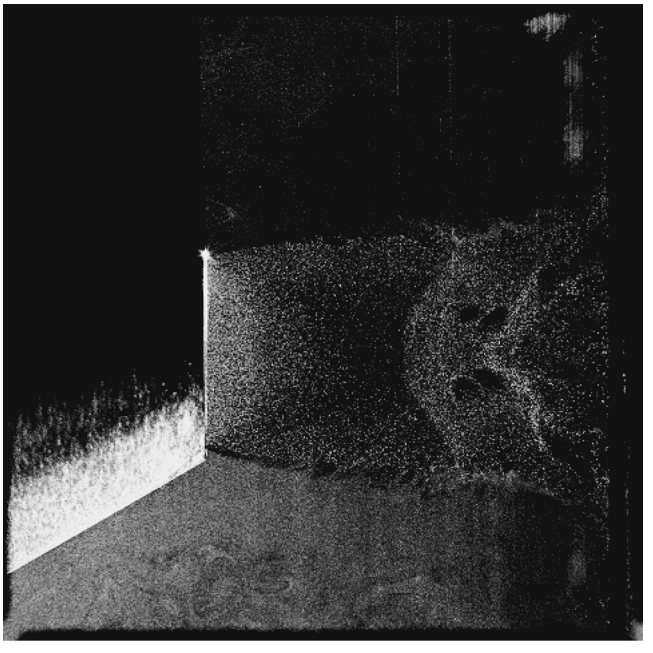

FIGURE 3. A typical image acquired in the DPIV studies.

The jet flow was seeded with 0.6 μm olive oil droplets produced by a TSI model 9306 Six-jet Atomizer. The seed injection point was 3 m upstream of the nozzle exit behind another set of screens in a 35.5 cm diameter settling chamber not shown in figure 1. A Vicount 5000 smoke generator with 0.2–0.3 μm smoke particles was used to seed the ambient air. Particle sizes were determined from manufacturer specifications. A typical image acquired from the DPIV studies is shown in figure 3.

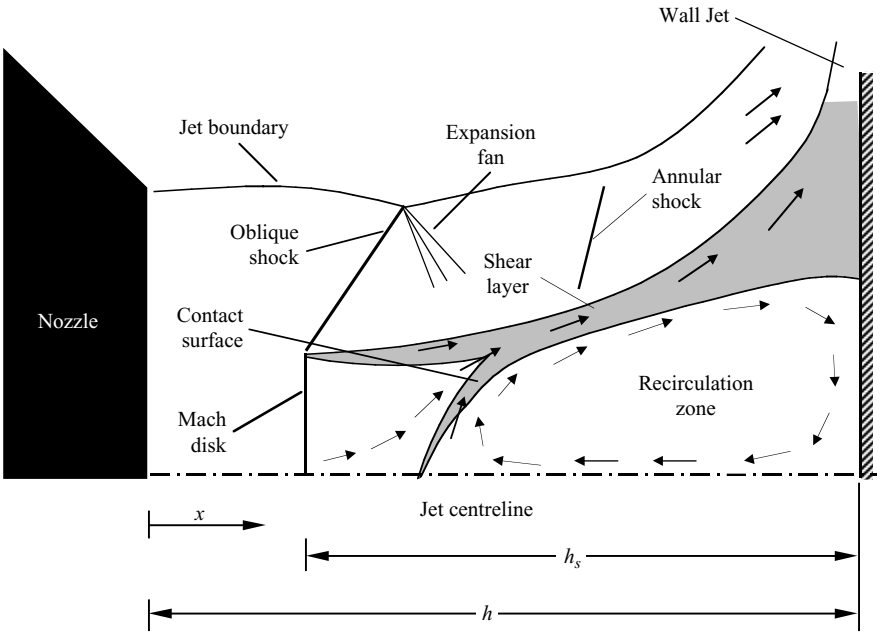

FIGURE 4. A schematic of the impingement region flow.

Phase-averaged and phase-delayed DPIV sequences for the oscillatory flow were constructed manually from a laser q-switch signal and a far-field microphone signal recorded simultaneously on an RC Electronics Datamax data acquisition unit. At each phase location, between 20 and 60 vector plots were averaged from a total of 800 image pairs acquired at each unsteady operating condition. For non-tone-producing plate locations (zones of silence), 400 image pairs were acquired and used to determine mean velocity characteristics. The full-scale errors given above were, therefore, reduced further through the averaging process. The DPIV images were processed with PIVPROC (see Wernet 1999), a NASA GRC-developed code. The processing is correlation-based and allows for subregion image shifting and multi-pass correlation to improve the spatial resolution of the resultant velocity vector maps. The first pass of the correlation uses a subregion size of 64×64 pixels with 50 % overlap. The second pass uses a 32×32 pixel subregion size, again with 50 % overlap. The resulting spatial resolutions of the velocity vector fields are 0.6 mm and 1.06 mm for the 80 mm and the 136 mm fields of view, respectively.

3. Description of the flow field

A schematic of the impingement region for the conditions discussed in this paper as adapted from the explanation given by Ginzburg *et al.* (1970) and Kalghatgi & Hunt (1976) is shown in figure 4. A shear layer forms between the subsonic flow in the central region of the jet behind the Mach disk and the supersonic flow in the peripheral regions of the jet behind the oblique shock. The total pressure lost behind the Mach disk is greater than that lost by the flow passing through the oblique shock, resulting in a low pressure at the plate centre and a pressure maximum further out on the plate. A portion of the flow near the plate cannot overcome the pressure maximum outboard of the central region of the plate and a recirculation zone forms.

NPR	*h/d*	PIV	Shadowgraph
	1.50	×	×
3.0	1.98	×	×
	2.88		×
	3.27		×
	1.38	×	×
3.4	2.20	×	
	3.00	×	×
	3.30		×
3.8	1.59	×	×
	2.06	×	×
	1.59	×	×
	2.02	×	×
	2.34	×	×
	2.60	×	
4.0	2.77		×
	3.00	×	×
	3.37	×	×
	3.67	×	×
	4.19	×	×
	4.70	×	×

TABLE 1. The test matrix used in the impinging jet study.

A contact surface forms between the recirculation zone and the flow behind the Mach disk. The flow passing through the Mack disk is diverted to the shear layer and away from the central regions of the jet.

An expansion fan appears at the intersection of the oblique shock and the jet boundary and balances the pressure along the jet boundary. The expansion waves intersecting the constant pressure boundary between the subsonic and the supersonic flow reflect as compression waves and merge to form an annular shock wave often observed in schlieren photographs (see Henderson 2002). When the wave system intersects the plate, in-phase reflection occurs followed by out-of-phase reflection at the wall jet boundary. Carling & Hunt (1974) found that the alternating pattern of compression and expansion waves persists well into the wall jet for several jet radii.

4. Experimental results

The operating conditions investigated and the types of flow measurements obtained in this investigation are shown in table 1. The majority of the results presented here are for NPR = 4.03 and *h/d* between 1.6 and 5.0, where *h* is the nozzle-to-plate spacing and *d* is the nozzle exit diameter, as these results represent those observed at other operating conditions when the dominant impinging tone is associated with a symmetrical jet oscillation and the plate is located within the first two shock cells of the free jet. A single impinging tone associated with a symmetrical oscillation mode often dominates the spectra for NPR between 3.7 and 4.5. For NPR below 3.7, multiple impinging tones often occur and are associated with symmetrical jet oscillations as well as helical or asymmetric jet disturbances. A more detailed description of the acoustic characteristics associated with supersonic impinging jets may be found in Henderson (2002).

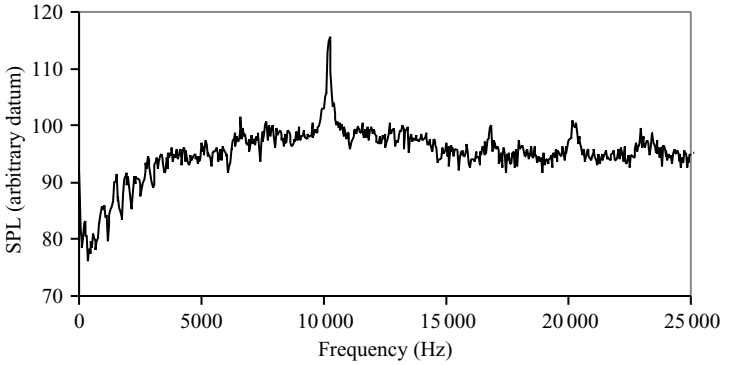

FIGURE 5. A typical power spectrum obtained at $h/d = 2.08$ and NPR = 4.03.

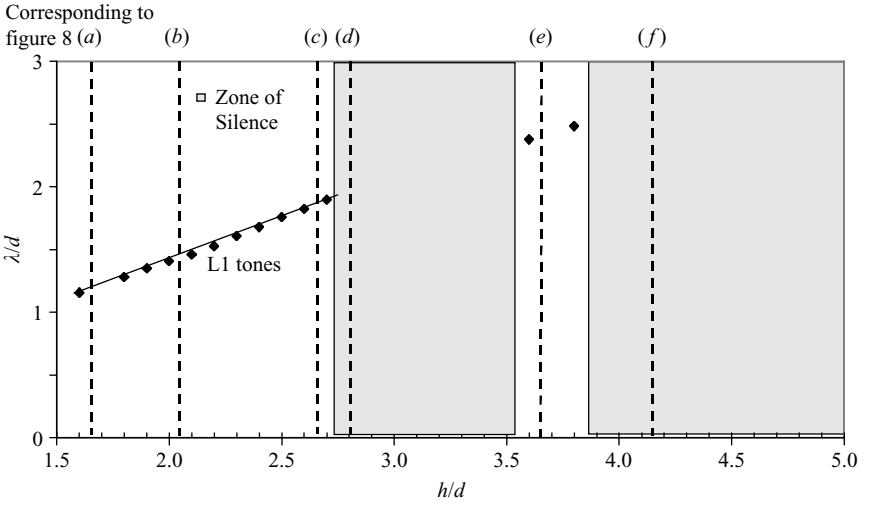

FIGURE 6. The normalized acoustic wavelength as a function of normalized nozzle-to-plate spacing for NPR = 4.03.

4.1. *Acoustic measurements*

A typical plot of the power spectrum obtained from a microphone located approximately 30° from the upstream jet axis at 0.5 m from the plate is shown in figure 5. An intense discrete frequency tone in addition to multiple harmonics is typically observed with the fundamental frequency often 20 dB above the local broadband noise.

A plot of the acoustic wavelength of the fundamental tone, λ, versus the nozzle-to-plate spacing is shown in figure 6. The tones indicated are associated with symmetrical jet oscillations and have been previously labelled L1 tones (see Henderson & Powell 1993). A 'zone of silence', where no tones are produced, exists when the plate is located between $h/d = 2.7$ and 3.5 and a second zone of silence begins around $h/d = 3.8$. The relationship between the results of these studies and the production of tones is discussed in the following sections. The dashed lines in the figure represent the plate spacings for which DPIV and shadowgraph studies were conducted.

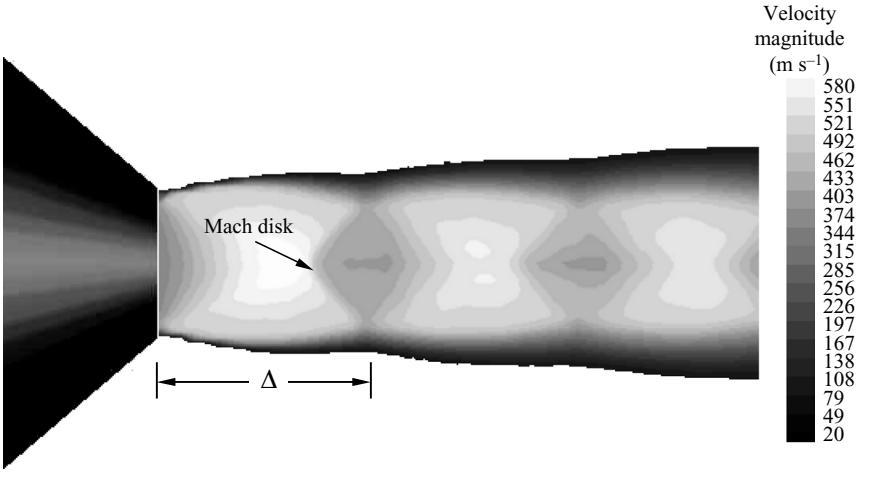

FIGURE 7. A contour map of the mean velocity magnitude for the free jet obtained at NPR = 4.03.

4.2. *Mean-flow measurements*

To understand better the connection between mean flow features and the production of tones, mean velocity fields for a range of nozzle-to-plate spacings were investigated. The studies were performed for tone-producing and non-tone-producing impinging jets as well as for the free jet. Velocity fields were obtained from DPIV studies by averaging 800 instantaneous vector fields for tone-producing conditions, and 400 instantaneous vector fields for non-tone-producing conditions. The estimated particle lag (see Melling 1997) behind the shock waves for the range of conditions presented in this investigation is between 1 and 3 mm. The Stokes number for the olive oil particles is roughly 2×10^{-10}. Although particle lag is expected to introduce velocity errors behind the shock waves, it is possible to obtain qualitative flow-field information in these regions of the flow. Velocity measurements in regions upstream of the shock waves are not affected by particle lag.

The free-jet mean velocity contours are shown in figure 7. The length of the first shock cell, Δ, is equal to $1.6d$, a value consistent with Prandtl's formula (1904) and Powell's (1988) observations. The first shock wave has a conical shape with the apex of the cone cut off by a Mach disk.

Mean impinging jet velocity magnitude contour plots for nozzle-to-plate spacings between 1.65 and 4.16 nozzle diameters are shown in figure 8. Velocity vectors for the impingement region flow are also shown in the figure. For conditions where the flow is unstable, L1 tones are produced. At small nozzle-to-plate spacings near where the L1 tone first occurs (see figure 8*a*), the flow in the central regions of the jet passes through a Mach disk while the flow in the peripheral regions of the jet is deflected through an oblique shock. As the nozzle-to-plate distance increases, the Mach disk moves downstream and the diameter of the Mach disk decreases (see figure 8*b*, *c*). The stand-off shock distance (h_s in figure 4) also increases with increasing nozzle-to-plate distance, resulting in a larger subsonic region in front of the plate. The contact discontinuities described in § 3 are also evident in figure 8(*b*, *c*). When the plate is moved within the first zone of silence (see figure 8*d*), the stand-off shock moves closer to the plate and the initial shock cell appears as it does in the free jet. The stand-off shock distance and velocity upstream of the stand-off shock wave are greatly reduced

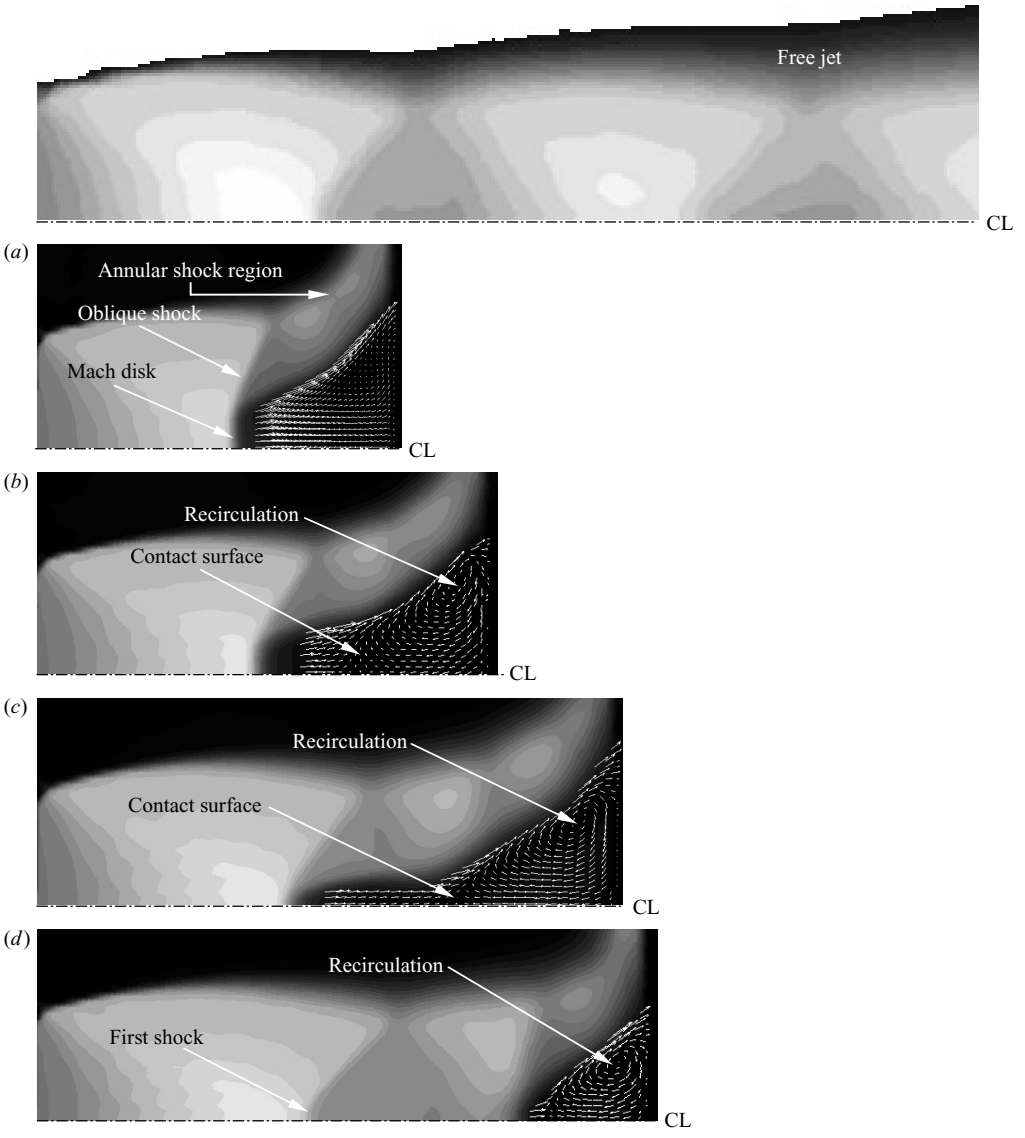

FIGURE 8(*a–d*). For caption see facing page.

from that observed in figure 8(*c*). (Semiletenko *et al.* (1974) also found that the addition of a second shock wave resulted in a stable non-tone-producing, jet.) As the nozzle-to-plate distance is increased further (see figure 8*e*), the stand-off shock moves downstream, the velocity upstream of the stand-off shock wave increases, the stand-off shock wave distance increases, and the tone reappears. The process repeats itself when the nozzle-to-plate distance is further increased, until the second zone of silence is reached: the first two shock cells of the free jet are complete and the stand-off shock moves closer to the plate. The Mach number upstream of the stand-off shock increases, and the stand-off shock wave distance again decreases.

Recirculation zones are observed in all of the impingement flows of figure 8 except that for $h/d = 1.65$, although for this condition averaged phase-delayed DPIV studies

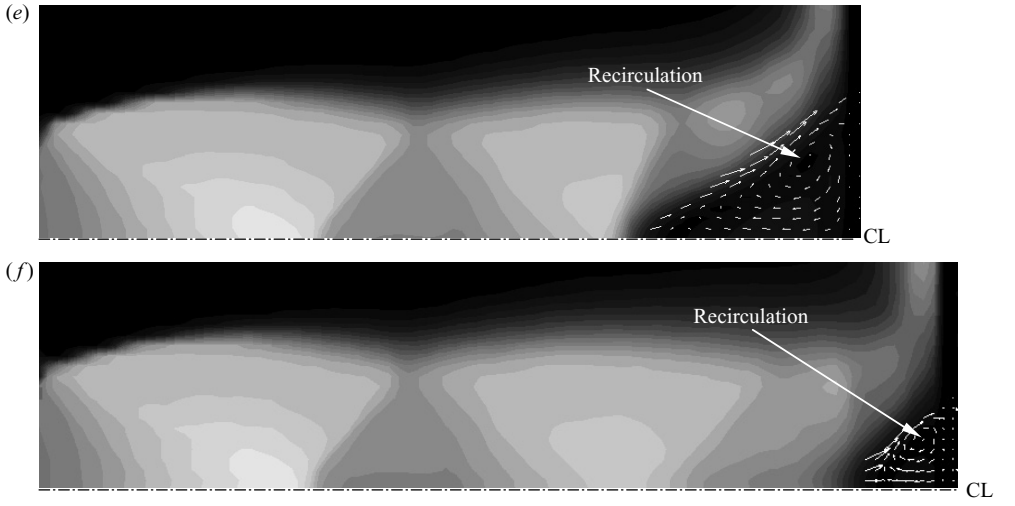

FIGURE 8. Contour maps of the mean velocity magnitude for the impinging jet obtained at an NPR = 4.03 and (*a*) *h*/*d* = 1.65 (unstable), (*b*) 2.08 (unstable), (*c*) 2.66 (unstable), (*d*) 2.80 (stable), (*e*) 3.65 (unstable) and (*f*) 4.16 (stable). The contour levels are the same as those shown in figure 7. The free jet has been included for comparison.

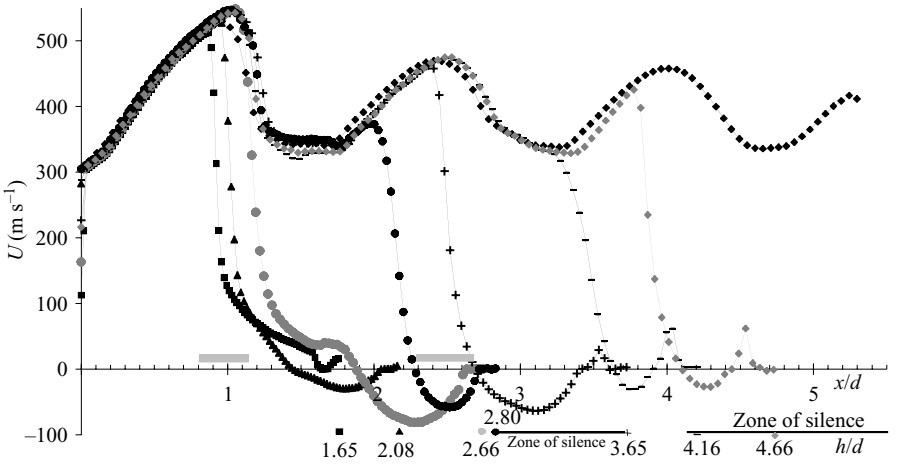

FIGURE 9. The streamwise centreline mean velocities for the free jet (◆) and the impinging jet obtained at NPR = 4.03 and *h*/*d* equal to 1.65 (■), 2.08 (▲), 2.66 (●), 2.80 (●), 3.65 (+), 4.16 (−), 4.66 (⬩). The stand-off shock locations for unstable flow are indicated by ▬.

showed that a recirculation zone appeared for at least a portion of the oscillation cycle. The presence of recirculation zones for both stable and unstable conditions indicates that the occurrence of recirculation zones does not guarantee instability.

Mean centreline axial velocity and Mach number (obtained by assuming adiabatic flow) for the free jet and the impinging jet are shown in figures 9 and 10, respectively. The distance, x, is measured from the nozzle exit as indicated in figure 4. Also shown in the figure are corresponding plate locations and the zones of silence for the impinging jet data.

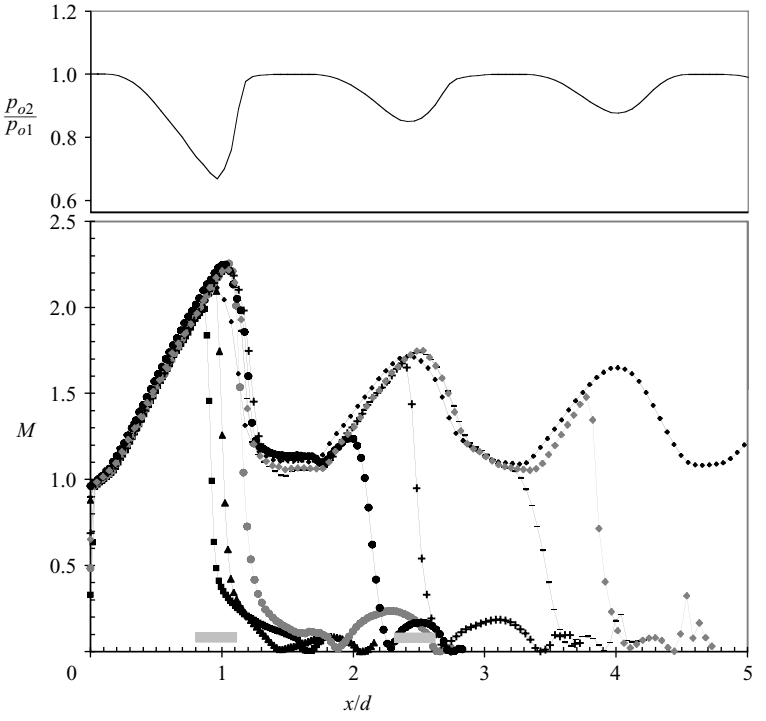

FIGURE 10. The centreline Mach numbers for the free and impinging jets obtained at NPR = 4.03 and the total pressure ratio, p_{o2}/p_{o1} (calculated from the free jet data) that would occur if a normal shock wave formed at the indicated value of x/d. The symbols are the same as in figure 9.

The occurrence of recirculation zones near the plate is evident in the centreline impinging jet velocity shown in figure 9 for all nozzle-to-plate spacings except $h/d = 1.65$. As the nozzle-to-plate distance increases from $h/d = 1.65$ to $h/d = 2.66$, figure 10 shows that the Mach number upstream of the stand-off shock increases slightly owing to the shock wave moving further downstream in the initial expansion region of the jet. The jet remains unstable until the nozzle-to-stand-off shock distance slightly exceeds the nozzle-to-Mach disk distance in the free jet, the stand-off shock jumps downstream, and the jet stabilizes. As the plate is moved further downstream to a nozzle-to-plate distance near $h/d = 3.65$, the Mach number upstream of the stand-off shock again increases and the jet once again becomes unstable. The jet remains unstable as the nozzle-to-plate distance is further increased until a point where the nozzle-to-stand-off-shock distance slightly exceeds the distance between the nozzle and second Mach disk in the free jet near $h/d = 4.16$, at which time the stand-off shock again jumps to a location closer to the plate and the jet stabilizes. Also shown in figure 10 is the ratio (calculated from the free-jet data) of the total pressure downstream of the shock, p_{o2}, and the total pressure upstream of the shock, p_{o1}, that would occur if a normal shock formed at the specified value of x/d.

The unstable regions for an impinging jet at an NPR = 3.4 are shown on the free-jet data in figure 11. The range of unstable shock locations is greatly reduced from that observed for an NPR = 4.03, possibly owing to a reduction in upstream Mach number with reduced NPR. Previous measurements (see Henderson 2002) made at an NPR = 4.5 indicate that the range of unstable shock locations increases significantly

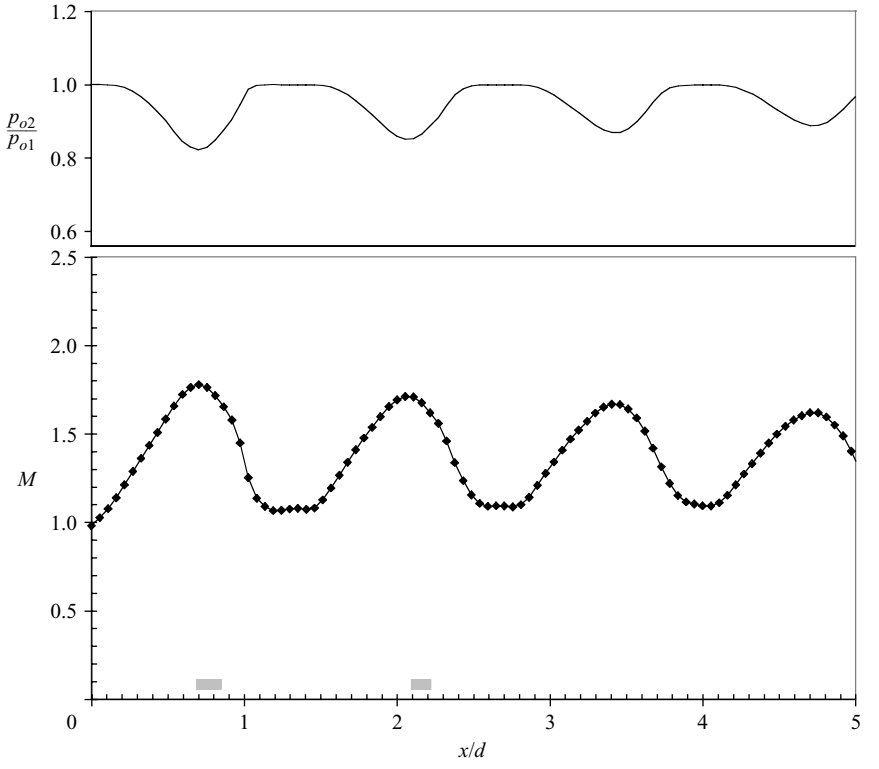

FIGURE 11. The centreline Mach numbers for the free jet obtained at NPR = 3.4 and the total pressure ratio, p_{o2}/p_{o1} (calculated from the free-jet data), that would occur if a normal shock wave formed at the indicated value of x/d. Unstable shock locations for the impinging jet are indicated by ▬.

with increasing NPR. The results of figures 10 and 11 indicate that instability occurs for flow conditions where a strong stand-off shock wave occurs in front of the plate. The exact upstream Mach number required for instability depends on NPR, although instability usually occurs when the stand-off shock forms in a location resulting in the greatest total pressure loss along the centreline of the jet. When the plate distance is increased such that the flow transitions to subsonic speeds through a weaker shock (lower upstream Mach number), the flow is stable and no tones are produced.

The unstable stand-off shock locations shown in figure 10 are in good agreement with those predicted by Kuo & Dowling (1996). A plot of the stand-off shock-wave distance, h_s, as a function of nozzle-to-plate spacing is shown in figure 12. For the range of nozzle-to-plate spacings investigated in this study, the stand-off shock-wave distance always exceeds $0.6d$ and recirculation zones are always present. These results are consistent with the computational results presented by Kuo & Dowling (1996).

4.3. *Phase-locked studies*

Phase-locked shadowgraph and DPIV studies were conducted to understand the oscillation cycle of the supersonic impinging jet and, in conjunction with the mean flow studies, to gain insight into the sound production mechanism and the feedback loop.

Phase-locked shadowgraph photographs of the impinging jet flow at $h/d = 2.08$ are shown in figure 13. The photos were taken at equally spaced times and show one

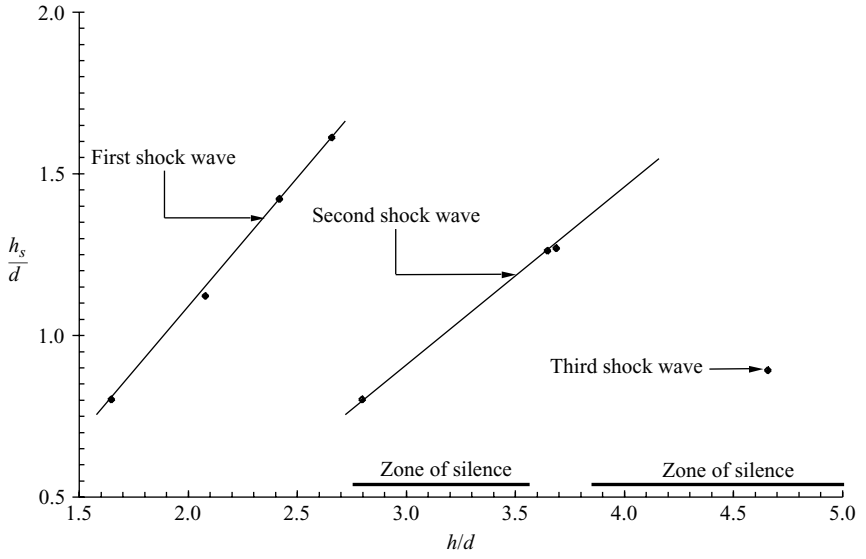

FIGURE 12. A plot of the normalized stand-off shock-wave distance as a function of normalized nozzle-to-plate spacing for NPR = 4.03.

complete period, T, of the jet oscillation cycle. Each photograph is the result of averaging two photographs taken at the same phase in the oscillation cycle. Results from similar studies conducted at other nozzle-to-plate spacings indicate that the main flow features observed in the photographs of figure 13 are representative of the dominant flow features of impinging jets producing L1 tones. Interior waves in the central region of the jet behind the Mach disk and an annular shock wave in front of the plate are visible in figure 13(a). The interior waves move downstream with progressing time as shown by the photographs taken at subsequent points in the oscillation cycle. Although it is difficult to see the annular shock motion in figure 13, animated movies developed from the sequenced shadowgraph photographs indicate that the annular shock wave moves toward the plate in figure 13(b) and becomes obscure (or perhaps disappears) in figures 13(c)–13(d). The annular shock reappears in figure 13(f) at an axial location further upstream than that in figure 13(a) and moves downstream with progressing time in figures 13(g) to 13(j). A strong sound wave emanating from the near-wall jet region is observed in the ambient flow in figure 13(e).

Ribner (1953), Ribner & Moore (1953) and Powell (1958) have shown that the interaction of a sound wave with a shock-wave produces shock-wave motion as well as a transmitted sound wave and an entropy wave downstream of the shock wave. The average convection speed of the interior waves, as determined from the phased shadowgraph photographs, is close to the speed of the flow in the subsonic region in front of the plate. Since it appears that these waves convect with the flow, they are most likely to be entropy waves. Powell also showed that the amplitudes of the transmitted sound waves and the shock-wave oscillations both increase as the Mach number upstream of the shock wave increases. This may explain the observation that oscillations occur when a strong stand-off shock wave occurs in front of the plate.

The addition of entropy waves in the instability model of Kuo & Dowling (1996) resulted in a strong resonance condition not obtained from earlier instability models that only allowed for sound waves in the impingement region. However, it is difficult

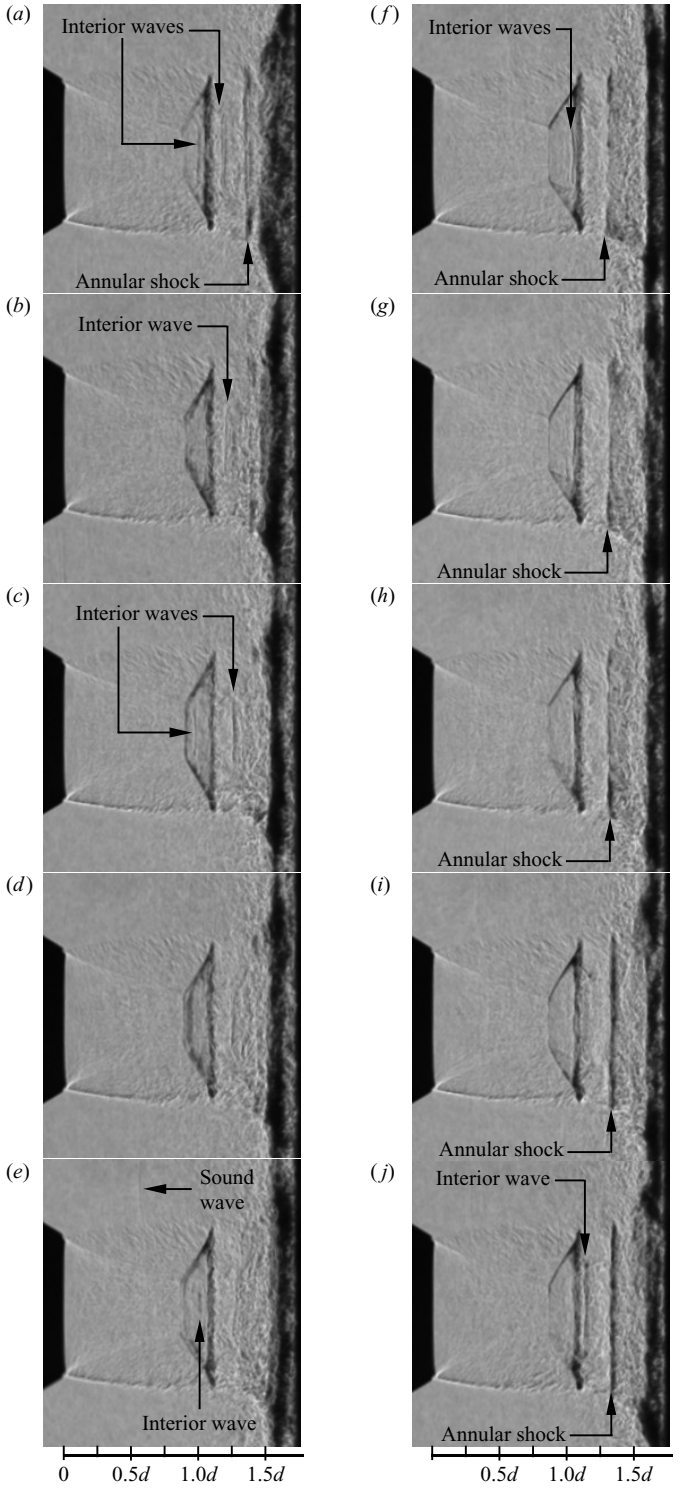

FIGURE 13. Phase-locked shadowgraph photographs obtained at NPR = 4.03, $h/d = 2.08$, and $\Delta t/T = 0.1$ apart.

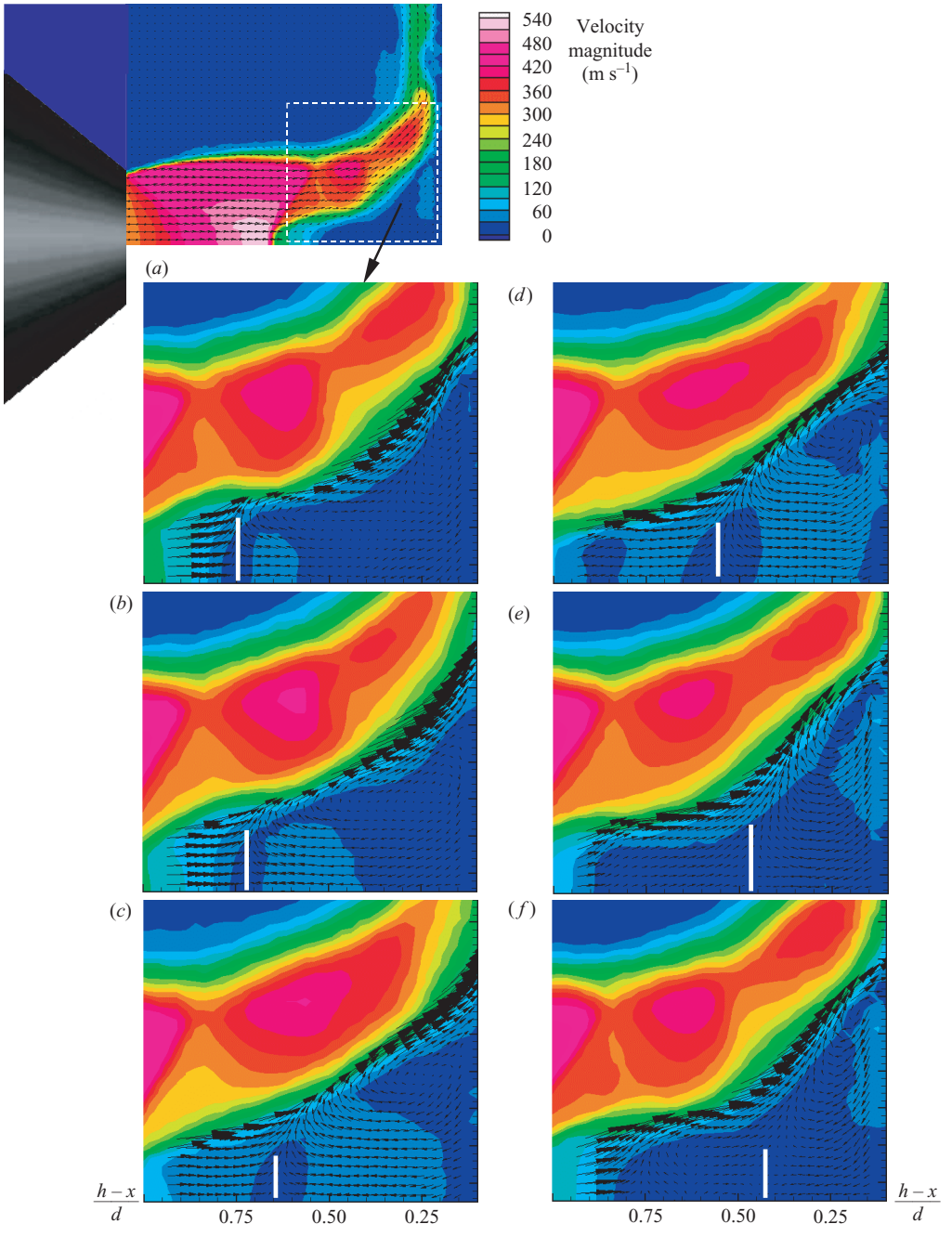

FIGURE 14. Phase-locked velocity magnitude plots for the impinging jet at NPR = 4.03, $h/d = 2.08$, and $\Delta t/T = 0.167$ apart. The vertical white lines indicate contact surfaces.

from the present investigation to determine the importance of the entropy waves to the sound production mechanism or the feedback loop.

Velocity magnitude and velocity vector maps of the recirculation region obtained from phase-locked DPIV studies are shown in figure 14 at six equally spaced times of a

complete oscillation cycle. Phase-locked and phase-averaged DPIV studies conducted at other nozzle-to-plate spacings where L1 tones are produced indicate that the oscillation cycle is quite similar for all nozzle-to-plate spacings before the first zone of silence and is represented well by the contour plots in figure 14. At the beginning of the oscillation cycle (see figure 14*a*), a recirculation zone exists in the subsonic flow close to the plate and a contact surface (represented by a vertical bar) occurs between the recirculating flow and the flow just downstream of the Mach disk. As time progresses, the contact surface moves downstream toward the plate and the recirculation zone moves toward the plate and outward radially, as can be seen from a detailed study of figure 14. The motion of the contact discontinuity and the recirculation zone coincide with axial oscillations of the Mach disk which are discussed in more detail in § 5. As the recirculation zones and associated contact surfaces move downstream, the shear layer and the outer supersonic flow distort. The alternating regions of compression move axially throughout the oscillation cycle. The two expansion regions merge in figures 14(*c*)–14(*d*) and are once again visible in figures 14(*e*)–14(*f*). The merging of the two expansion regions is probably associated with the disappearance of the annular shock wave in the shadowgraph photographs of figure 13.

Figure 15 shows the wall jet at the same points in the oscillation cycle as those in figure 14. The frames are centred at approximately 2.6 jet radii from the jet centreline. Pronounced oscillations are seen to occur in the wall jet and are the result of the motion of the recirculation zones in the inner subsonic flow and the resulting oscillations of the compression and expansion regions in the peripheral supersonic flow. At the beginning of the oscillation cycle (see figure 15*a*, *b*), the ambient flow is drawn toward the wall, as depicted by the large white arrows. The ambient flow is tangent to the wall in figure 15(*c*) and is directed away from the wall in figure 15(*d*). The ambient flow once again becomes tangent to the wall in figure 15(*e*) and is again drawn toward the wall in figure 15(*f*) to complete the oscillation cycle. The impingement tones are most probably produced in the wall jet with fluctuations of the jet boundary acting as a simple source distributed over an annulus centered at $2.6R$ from the jet centreline. Additional evidence of the sound source location is shown in figure 16 where contours are plotted for the difference in the mean velocity and the velocity associated with a single phase of the oscillations in figure 16(*a*) and a shadowgraph photograph is shown in figure 16(*b*). Acoustic waves in the exterior flow surrounding the jet appear to originate from the near-wall region of the jet at a radial location of $2.6R$ from the jet centreline.

5. The feedback cycle and sound-production mechanism

Results from previous investigations indicate that large-plate impingement tones are part of a feedback loop to the nozzle (see Henderson & Powell 1993). Results from the present investigation indicate that disturbances created at the nozzle lip travel downstream and interact with the shock wave, causing the shock wave to displace and producing entropy waves, sound waves and shear waves behind the shock. As the shear waves travel downstream in the shear layer, the peripheral supersonic flow distorts resulting in the motion and eventual disappearance of the annular shock wave. The distortions of the inner shear layer and the peripheral supersonic flow lead to oscillations in the wall jet at a radial distance of $2.6R$ from the jet centreline, where R is the exit radius of the nozzle. The oscillating jet boundary produces sound that propagates back to the nozzle lip and produces flow disturbances, thus closing the feedback loop.

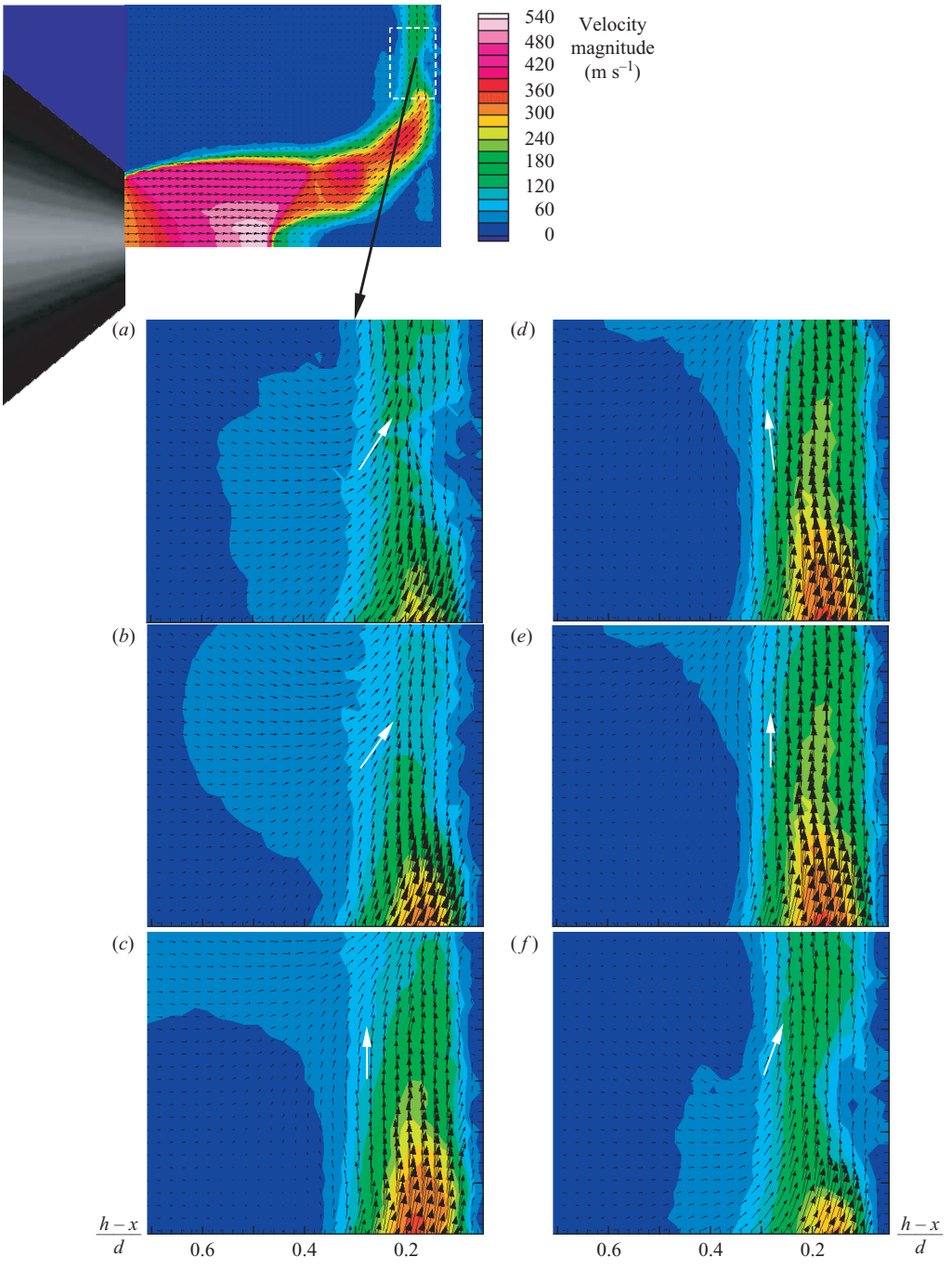

FIGURE 15. Phase-locked velocity magnitude plots for the impinging jet at NPR = 4.03, $h/d = 2.08$, and $\Delta t/T = 0.167$ apart.

Contour and vector plots of the difference between the mean velocity field and the velocity at each of six phase-locked locations were developed (see figure 17) to understand better the oscillation cycle in the impingement region. A schematic of

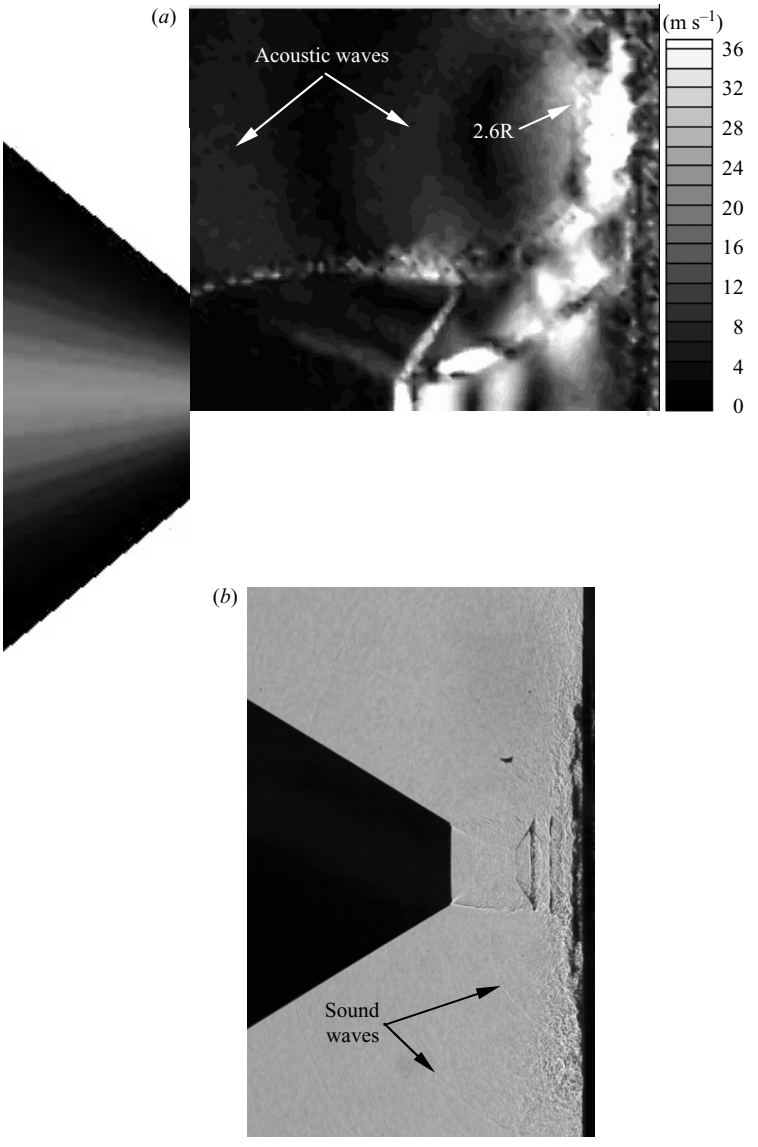

FIGURE 16. (*a*) The subtracted velocity vector field obtained from PIV data and (*b*) a shadowgraph photograph. Both images are for NPR = 4.03 and $h/d = 2.08$.

the dominant flow features observed in figure 17 is shown in figure 18. The plot in figure 17(*a*) is located at the same position in the oscillation cycle as the contour plot in figure 14(*a*). As the Mach disk oscillates axially, regions of unsteady rotating velocity are generated behind the Mach disk. They move downstream in the shear layer between the subsonic flow behind the Mach disk and the supersonic flow in the peripheral regions of the jet as time progresses. The rotating regions draw fluid into, and away from, the shear layer as indicated by the straight lines in figures 17 and 18. The arrows indicate the direction of fluid motion. The contact surface, indicated by a red vertical line in figure 17, moves downstream with the rotational velocity components. At the points in the oscillation cycle corresponding to the subtracted

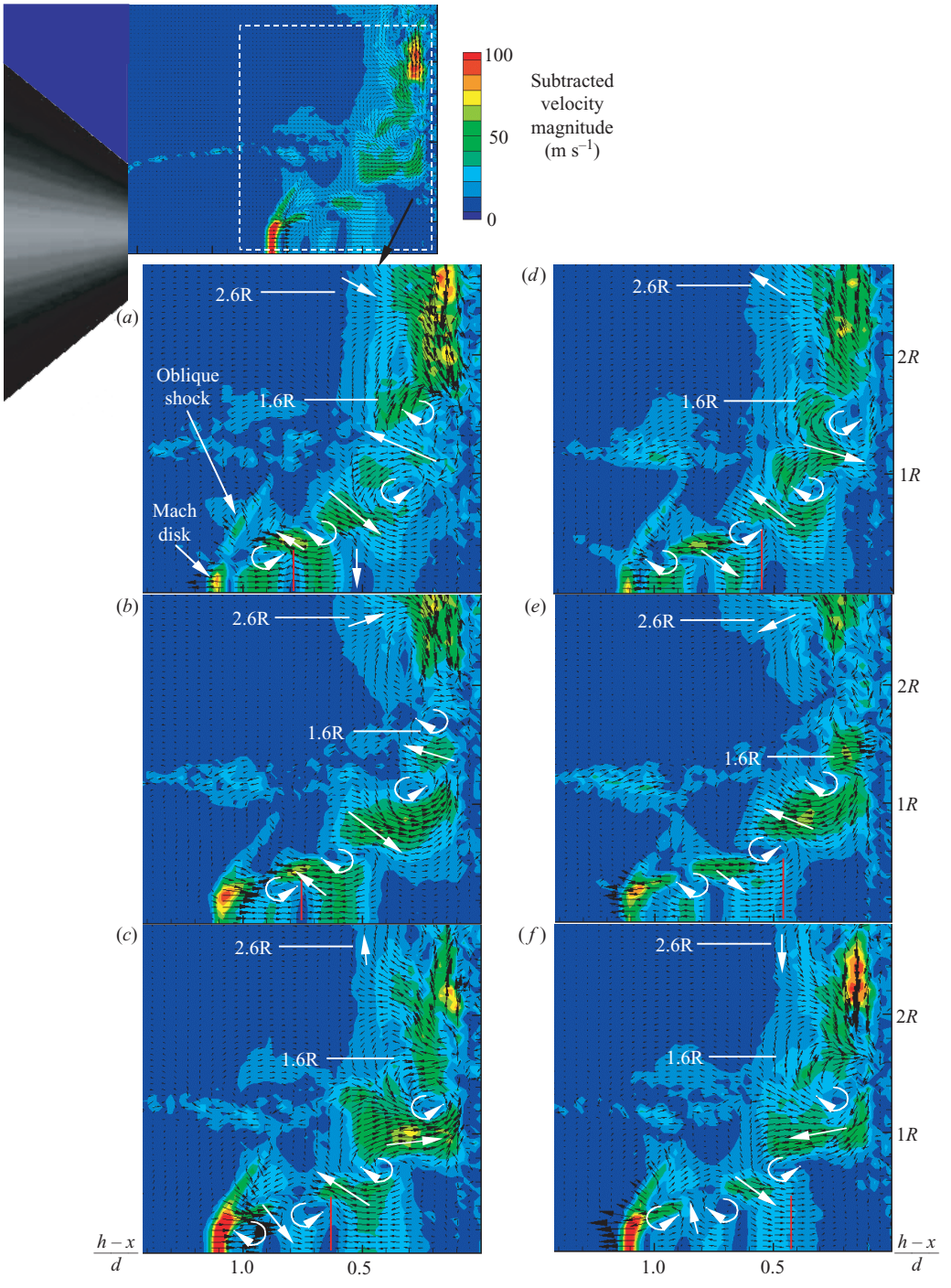

FIGURE 17. The subtracted velocity vector fields obtained at NPR = 4.03, $h/d = 2.08$, and $\Delta t/T = 0.167$. The white arrows indicate the direction of the velocity in the corresponding fluid region. The red vertical line indicates the location of the contact discontinuity shown in figure 14.

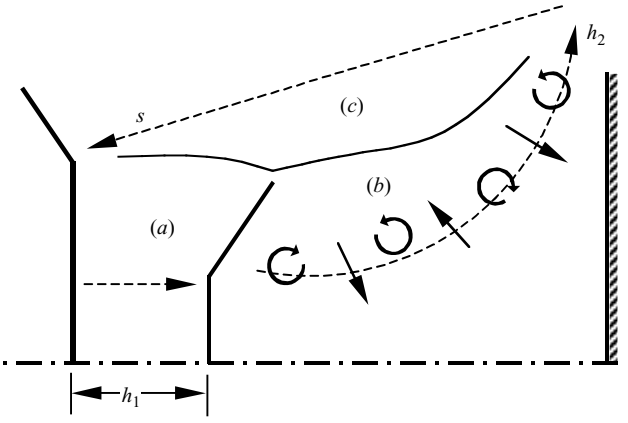

FIGURE 18. A schematic of the subtracted velocity vector fields shown in figure 17.

fields in figures 17(*c*) and 17(*e*), the fluctuating rotational velocity components collapse in the wall jet near a radius of $1.6R$ ($0.8d$) from the jet centreline. Pronounced velocity fluctuations occur in the outer regions of the wall jet at approximately $1.2d$ from the centreline as a result of the motion and collapse of the rotational velocity components. The unsteady fluid motion in the shear layer also significantly affects the flow adjacent to the wall jet. The flow at $2.6R$ ($1.3d$) from the jet centreline is drawn into the wall jet in figures 17(*a*) and 17(*b*), becomes tangent to the wall jet in figure 17(*c*), is directed away from the wall jet in figures 17(*d*) and 17(*e*), and once again becomes tangent to the wall jet in figure 17(*f*). The wall jet oscillations at $2.6R$ create a fluctuating mass flow rate along the jet boundary as the ambient flow is drawn into, then directed away from, the wall jet. Unsteady plate pressure measurements obtained by Henderson (2002) show a secondary pressure maximum at approximately $1.6R$ for a nozzle-to-plate spacing of $h/d = 1.74$ which is most probably associated with the changes in the unsteady flow noted above. The sound waves observed in the surrounding ambient flow are produced by the oscillations of the wall jet boundary with the boundary acting as a distributed simple source. The sound source model proposed here is similar to that developed for small plates by Glaznev (1977) where the wall jet was modelled as an oscillating membrane.

6. Conclusions

A detailed investigation of the oscillatory flow field of the impinging jet was conducted using phase-locked DPIV and shadowgraph photography. Periodic axial oscillations of the stand-off shock wave were accompanied by oscillations of the recirculation zones in the subsonic impingement flow and oscillations of the compression and expansion regions in the peripheral supersonic flow near the plate. The impingement flow oscillations give rise to a periodic pulsing of the wall jet boundary resulting in the production of discrete frequency sound.

Instability of the jet is not guaranteed by the occurrence of recirculating zones in the impingement flow. Both stable and unstable impinging jets have recirculation zones. The stability condition of the jet appears to depend on the strength of the stand-off shock and the velocity gradient in front of the shock. For the conditions investigated in this study, instability (and tonal production) occurs when the Mach number upstream of the stand-off shock wave is slightly greater than that of the fully

expanded Mach number (resulting in the production of L1 tones when the stand-off shock is located in the second half of the expansion region of the first or second free-jet shock cell). Zones of silence appear when the stand-off shock is 'close' to the plate.

A detailed description of the feedback loop was developed using phased velocity fields subtracted from the mean velocity fields. The progression of disturbances through the shear layer between the subsonic impingement flow and the supersonic peripheral flow and the resulting oscillations of the wall jet flow were documented.

The authors thank Kenneth Weiland for his assistance with the shadowgraph photography and Wentworth John and Garret Clayo for their assistance with the DPIV studies. The authors also thank Tom Norum for many helpful discussions. This work was funded under the Quiet Aircraft Technology program.

REFERENCES

Alvi, F. S. & Iyer, K. G. 1999 Mean and unsteady flowfield properties of supersonic impinging jets with lift plates. *AIAA* 99-1829.

Alvi, F. S., Ladd, J. A. & Bower, W. W. 2002 Experimental and computational investigation of supersonic impinging jets. *AIAA J.* **40**, 599–609.

Arunajatesan, S. & Sinha, N. 2002 Large eddy simulations of supersonic impinging jet flow fields. *AIAA* 2002-4287.

Carling, J. C. & Hunt, B. L. 1974 The near wall jet of a normally impinging, uniform, axisymmetric, supersonic jet. *J. Fluid Mech.* **66**, 159–176.

Donaldson, C. duP. & Snedeker, R. S. 1971 A study of free jet impingement. Part 1. Mean properties of free and impinging jets. *J. Fluid Mech.* **45**, 281–319.

Elevarasan, R., Krothapalli, A., Venkatakrishnan, L. & Lourenco, L. 2002 Suppression of self-sustained oscillations in a supersonic impinging jet. *AIAA J.* **39**, 2366–2373.

Elavarasan, R., Lourenco, L., Venkatakrishnan, L. & Krothapalli, A. 1999 Application of PIV to large scale STOVL supersonic jet facility. *AIAA Paper* A99-16176.

Ginzburg, I. P., Semiletenko, B. G., Terpigor'ev, V. S. & Uskov, V. N. 1970 Some singularities of supersonic jet interaction with a plane obstacle. *Inzhenerno-Fizicheskii Z.* **19**, 412–417. (Eng. trans. *J. Engng Phys.* **19**, 1081–1084 (1973)).

Ginzburg, I. P., Semiletenko, V. N. & Uskov, V. N. 1975 Experimental study of underexpanded jets impinging normally on a plane baffle. *Fluid Mech. Sov. Res.* **4**, 93–105.

Glaznev, V. N. 1977 Sound field of an underexpanded supersonic jet impinging on a barrier. *Sov. Phys. Acoust.* **23**, 142–145.

Gummer, J. H. & Hunt, B. L. 1974 The impingement of non-uniform, axisymmetric supersonic jets on a perpendicular flat plate. *Israel J. Technol.* **12**, 221–235.

Henderson, B. 1993 Sound source mechanisms of the axisymmetric supersonic impinging jet. PhD thesis, University of Houston.

Henderson, B. 2002 The connection between sound production and jet structure of the supersonic impinging jet. *J. Acoust. Soc. Am.* **111**, 735–747.

Henderson, B., Bridges, J. & Wernet, M. 2002 An investigation of the flow structure of tone producing supersonic impinging jets. *8th AIAA/CEAS Aeroacoustics Conf. Breckenridge, Co. AIAA Paper* 2002-2529.

Henderson, B. & Powell, A. 1993 Experiments concerning tones produced by an axisymmetric choked jet impinging on a flat plate. *J. Sound Vib.* **168**, 307–326.

Henderson, B. & Powell, A. 1996 Sound-producing mechanisms of the axisymmetric choked jet impinging on small plates: the production of primary tones. *J. Acoust. Soc. Am.* **99**, 153–162.

Henderson, B. & Powell, A. 1997 The use of an array to explain the sound characteristics of secondary small plate tones produced by the impingement of an axisymmetric choked jet. *J. Acoust. Soc. Am.* **102**, 1454-1462.

Iwamoto, J. & Deckker, B. E. L. 1981 Development of flow field when a symmetrical underexpanded sonic jet impinges on a flat plate. *J. Fluid Mech.* **113**, 299–313.

KALGHATGI, G. T. & HUNT, B. L. 1976 The occurrence of stagnation bubbles in supersonic jet impingement flows. *Aero. Q.* **27**, 169–185.

KROTHAPALLI, A., RAJKUPERAN, E., ALVI, F. & LOURENCO, L. 1999 Flow field noise characteristics of a supersonic impinging jet. *J. Fluid Mech.* **392**, 155–181.

KUO, C. & DOWLING, A. P. 1996 Oscillations of a moderately underexpanded choked jet impinging upon a flat plate. *J. Fluid Mech.* **315**, 267–291.

MELLING, A. 1997 Tracer particles and seeding for particle image velocimetry. *Meas. Sci. Technol.* **8**, 1406–1416.

MORCH, K. A. 1964 A theory for the mode of operation of the Hartmann air jet generator. *J. Fluid Mech.* **20**, 141–159.

MORCH, K. A. 1973 On the impingement of a composite jet. *The Technical University of Denmark Rep.* 47.

NAKATOGAWA, T., HIRATA, M. & KUKITA, Y. 1971 Disintegration of a supersonic jet impinging normally on a flat plate. *J. Spacecraft* **8**, 410–411.

POWELL, A. 1953 On edge tones and associated phenomena. *Acustica* **3**, 233–243.

POWELL, A. 1958 One-dimensional treatment of weak disturbances of a shock wave. Fluid Motion Sub-committee, Aeronautical Research Council (UK).

POWELL, A. 1988 The sound-producing oscillations of round underexpanded jet impinging on normal plates. *J. Acoust. Soc. Am.* **83**, 515–533.

PRANDTL, L. 1904 Uber die stationarem wellen in einem gasstrahle. *Phys. Z.* **5**, 599–601.

RIBNER, H. S. 1953 Convection of a pattern of vorticity through a shock wave. *NACA TN* 2864.

RIBNER, H. S. & MOORE, F. K. 1953 Unsteady interaction of disturbances with a shock wave, with applications to turbulence and noise. Presented at the Heat Transfer and Fluid Mechanics Institute, Palo Alto, CA.

SEMILETENKO, B. G., SOBKOLOV, B. N. & USKOV, V. N. 1974 Features of unstable interaction between a supersonic jet and infinite baffle. *Fluid Mech. Sov. Res.* **3**, 90–95.

WERNET, M. P. 1999 Fuzzy logic digital PIV processing software. *18th Intl Congress on Instrumentation for Aerospace Simulation Facilities (ICIASF) Conf. Toulouse, France.*